Stability enhancement of a low initial density hollow gas-puff z pinch by e^- beam preionization

E. Ruden, H. U. Rahman,[a] A. Fisher, and N. Rostoker
Physics Department, University of California, Irvine, California 92717

(Received 21 July 1986; accepted for publication 23 October 1986)

e^- beam preionization of the initial gas column of the hollow gas-puff z pinch at the University of California, Irvine is shown to decrease the amplitude of Rayleigh–Taylor instabilities which disrupt the imploding plasma shell of low initial density ($<1\times10^{17}$ cm^{-3}) helium pinches. A 5-ns pulsed nitrogen laser Mach–Zehnder interferometer compares the plasma density profile at various times during the implosion for preionized and unpreionized pinches. Also, a *B*-dot current probe compares the plasma induction fluctuations of the pinched state. Numerical calculations of the effects of the Rayleigh–Taylor growth for our geometry are discussed.

INTRODUCTION

Low initial density ($<1\times10^{17}$ cm^{-3}) He gas columns were pinched with the UCI *z* pinch with density profiles recorded at various times during the implosion by use of a 5-ns pulsed N_2 laser Mach–Zehnder interferometer.[1,2] Implosions of columns which are partially ionized with an e^- beam prior to gas breakdown are compared to implosions for which no e^- beam is applied. It is shown that, at these densities, preionization significantly decreases the amplitude of instabilities, presumably of R–T (Rayleigh–Taylor) origin, which grow during the implosion. A *B*-dot loop measuring total *z* current indicates that, as a result, the plasma pinches to a smaller volume.

The pressure balance condition for a Bennet pinch is[3]

$$(Z+1)N_iKT=\mu_0I^2/8\pi, \tag{1}$$

where N_i is the number of ions per unit length in the *z* direction, Z is the average degree of ionization, T is the plasma temperature, and I is the plasma current when the pinched state occurs. The motivation for going to lower initial densities stems, in general, from the expectation that, given a maximum I determined by the machine, higher temperatures may be achieved by decreasing N_i, as shown by the above Bennett condition. The pinched state can be delayed until the current has time to rise to its maximum value by increasing the initial plasma radius R_0 when lowering N_i. Even to the extent that the (quasistatic) Bennet condition is inapplicable, higher temperatures are predicted for lower values of N_i since roughly the same mechanical work performed on the plasma by the magnetic field will be channeled into the thermal motion of fewer particles by shock heating when the plasma collides with itself at the *z* axis.

Unfortunately, the gas column will not break down below a critical density. Even at higher densities, breakdown is delayed. When the time scale of the breakdown is of the same order as that of the implosion, large amplitude initial perturbations in the plasma column's shape result. This may be inferred from interferograms showing the amplified form of these perturbations midway into the explosion.

EXPERIMENT

Illustrated in Fig. 1, the *z*-pinch circuit consists of a 12-μF capacitor bank charged to -30 kV and discharged across the anode–cathode gap by parallel sparkgaps through a total inductance of 53 nH giving a quarter-cycle current rise time of 1.25 μs. The gas is injected as a hollow cylindrical shell of radius $R_0=2$ cm through a brass nozzle/cathode (Fig. 2) by a fast gas valve.[4] The gas passes through a gas-transparent stainless-steel honeycombed anode 0.7 cm thick that is 1.2 cm from the nozzle. The preionization circuit (Fig. 1) consists of a 0.3-μF capacitor charged to -30 kV and discharged by a sparkgap through a 100-Ω resistor to a 2-cm-radius circular carbon bristle brush[5] which lies 1 cm below the honeycombed anode directly in the path of the gas as it exits the anode. The e^- emitting brush consists of thousands of 7-μm graphite fibers confined by two twisted strands of wire as in a pipe cleaner. The resultant double-twisted strand, with fibers pointing radially outward and trimmed to uniform length of about 5 mm, is then bent into a circle of the same radius as the gas column.

The brush circuit is fired about 100 ns prior to discharging the main capacitor bank, at which time the brush current reaches $I_e\approx100$ A. This would result in a 10-kV voltage drop across the 100-Ω resistor leaving a 20-keV e^- beam. Since the (grounded) honeycomb is highly transparent to particles, a large fraction of the e^-'s should pass through creating a hollow cylindrical beam superimposed on the gas column. With an ionization cross section σ for He of $\sim10^{-18}$ cm^2 at 20 keV (Ref. 6) and a current density $J\sim10$ A cm^{-2} for a time $\Delta t\sim10^{-7}$ s, the fraction of He ionized should be $F_i=J\sigma\Delta t/e\sim10^{-5}$ for gas densities less than $\sim10^{18}$ cm^{-3}. No improvements were observed by increasing Δt.

The relative timing of the gas valve, preionization circuit, and the main capacitor bank is accomplished as follows. Initially, the valve is triggered manually. The signal from a gas breakdown pin near the valve opening is delayed by about 0.35 ms and then branched to two parallel delay boxes. One box has a 1.0 μs delay and is used to trigger the preionization circuit. The other box is set to 1.15 μs and triggers the sparkgaps for the main bank. The relative timing between

[a] University of California, Riverside, Dept. Physics, Riverside, CA 92521.

 0021-8979/87/041311-06$02.40

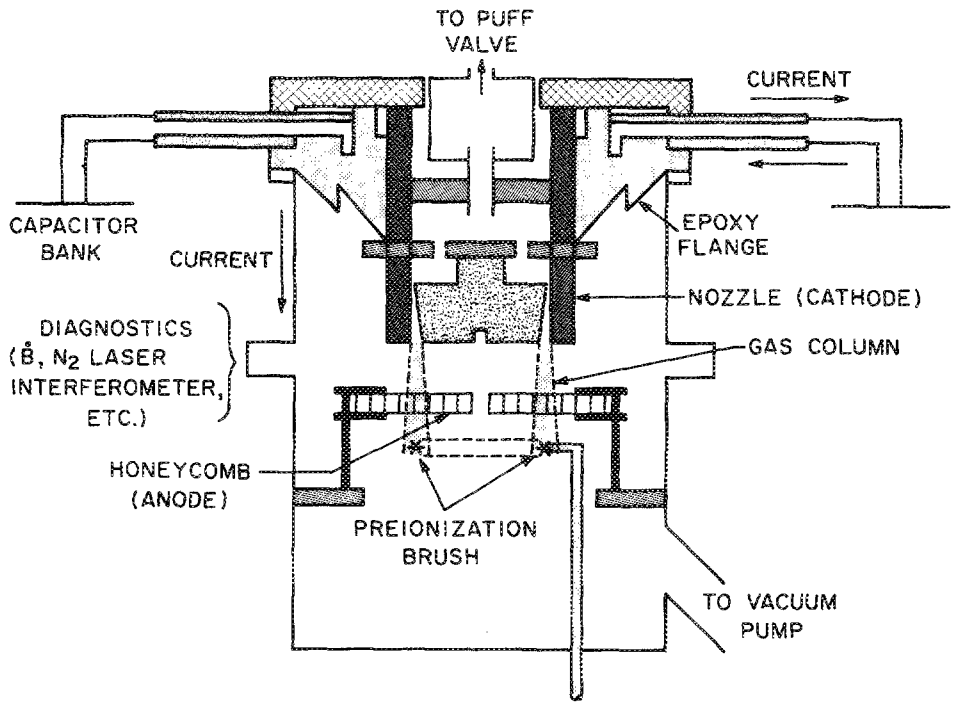

FIG 1. Schematic of gas puff z pinch.

the preionization current and the z-pinch current is more accurately determined by direct comparison of their respective current probe signals.

The primary diagnostic for this experiment is a 3371 Å N_2 laser Mach–Zehnder interferometer with 5-ns FWHM pulse width. One path of the split beam traverses the plasma column perpendicular to the z axis. When recombined with the unperturbed path, each fringe shift in the resultant interference pattern correspond to a free e^- density line integral along the laser path of 6.6×10^{17} m^{-2}. Figures 3(a)–3(c) are contrast-enhanced interferograms of different implosions at consecutively smaller radii for unpreionized gas columns. Corresponding data are shown in Figs. 3(d)–3(g) for preionized columns. The output of the delay box used to trigger the main capacitor bank is further delayed to provide a trigger for the N_2 laser used for the interferometer. A fast photodiode signal superimposed on the signal from the B-dot pinch current probe is used to measure the time between the laser pulse and the final pinched state so that an appropriate delay can be estimated. The accuracy, however, is insufficient to distinguish between the different interferograms of Fig. 3.

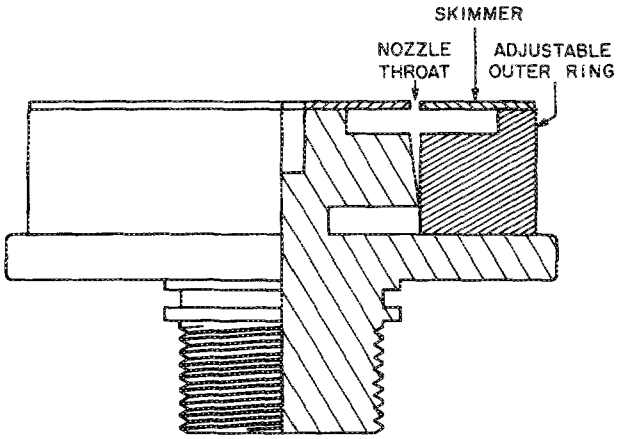

FIG. 2. Nozzle configuration.

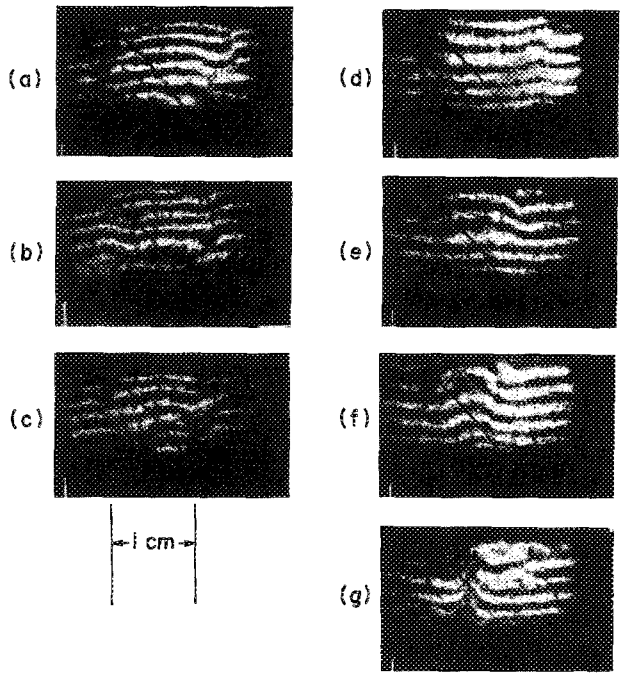

FIG. 3. N_2 laser interferograms.

DISCUSSION

The method we use to determine the phase shift of the nth fringe of a given interferogram is to manually digitize the curve $z = C_n(y)$ tracing the crest of constructive interference and compare it to the corresponding curve $z = B_n(y)$ of a "blank" interferogram for which no phase is present. Here, the z direction is just that of pinch's z axis and the y direction is normal to this in the plane of the film and is approximately parallel to the (almost straight) blank fringes. The fringe shift is taken to be

$$S_n(y) = \frac{C_n - B_n}{|\langle B_n - B_{n\pm1}\rangle|}, \tag{2}$$

where "$\langle\ \rangle$" means to average over y. S_n is negative for Figs. 3(a)–3(c), but this is of no physical significance. The z coordinate of the plasma producing this shift is taken to be $\langle B_n \rangle$. Since $S_n(y)$ is proportional to the projection of the plasma's free-electron-density profile onto the $y-z$ plane, an electron density n_e radially symmetric about the z axis will produce an S_n symmetric in y. Although the converse (y symmetry in S_n implies r symmetry in n_e) is not necessarily true, it is strongly indicated for our geometry since the anode and nozzle/cathode are radially symmetric.

The scale of distance is shown in the bottom left-hand corner of Fig. 3. Half the horizontal distance between the points of a fringe that just begin to deflect from the blank fringe is one way to estimate the radius of the plasma shell at that z coordinate. Based on this, the radii for Figs. 3(a)–3(c) are 0.75 ± 0.1, 0.65 ± 0.1, and 0.55 ± 0.1 cm, respectively. For Figs. 3(d)–3(g), the radii are 0.70 ± 0.05, 0.48 ± 0.1, 0.3 ± 0.05, and 0.2 ± 0.02 cm. The deviation terms refer to the spread for the different fringes. No unpreionized interferograms were identified with radii as small as those of Figs. 3(f) or 3(g).

For Figs. 3(b) and 3(c), the spread in radii, if measured from the z axis, is actually larger since there is a loss of symmetry about this axis not reflected in the above deviation terms. Figure 3(a), although, represents the stage of the implosion where perturbations are apparent but sufficient radial symmetry remains for an Abel inversion[7] to yield an approximation for the e^- density as a function of radius [Fig. 4(a)]. A corresponding inversion of Fig. 3(d) (preionized) is presented for comparison [Fig. 4(b)]. Although radial symmetry is greatly enhanced by preionization, as indicated by the bilateral symmetry of Figs. 3(d)–3(g), significant mass transport toward the nozzle (up) is apparent in Figs. 3(d)–3(f). This transport manifests itself as a growing disparity in the degree of shift between top and bottom fringes. This effect will be treated in the context of linear R–T growth calculation at the end of the paper.

Independent evidence that preionized pinches achieve smaller radii comes from the observation that the amplitude of the "dip" in B-dot probe signals are larger with preionization (Fig. 5). The B-dot probe measures dB_θ/dt (and therefore dI/dt) far away from the plasma (~ 15 cm). The probe is primarily used to record the time of the pinch. However, it is also a qualitative indicator of the relative degree of compression of different pinches with similar timing because of the coupling of the plasma's current I to its inductance L_p

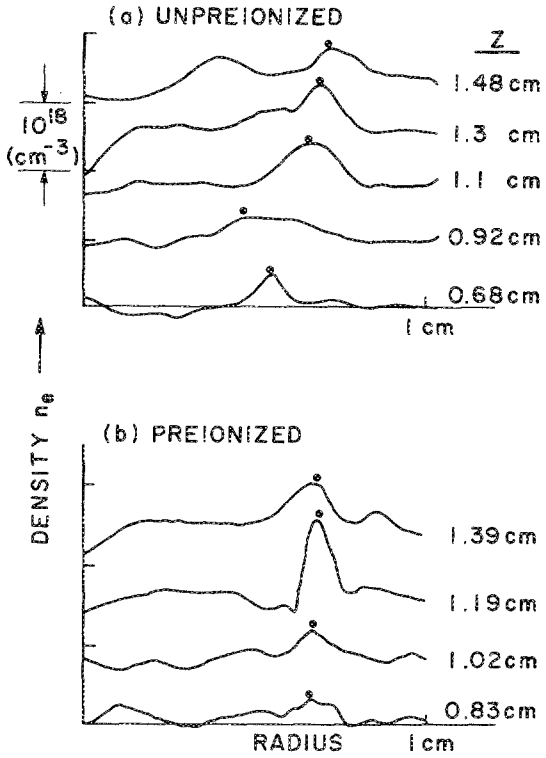

FIG. 4. Abel inversions of interferograms.

through the first-order circuit equations,

$$V = -\frac{d(IL)}{dt}; \quad I = -C\frac{dV}{dt}. \tag{3}$$

Here, V and C are the capacitor bank's voltage and capacitance, respectively, and L is the total circuit inductance (transmission line plus L_p). Imploding to a smaller radius will produce a greater fluctuation in L_p and, therefore, I. B-dot traces also show that the current rise for unpreionized columns start 200–300 ns later than with preionized columns [Figs. 5(a) and 5(b) start sweeping at different times relative to the sparkgap trigger].

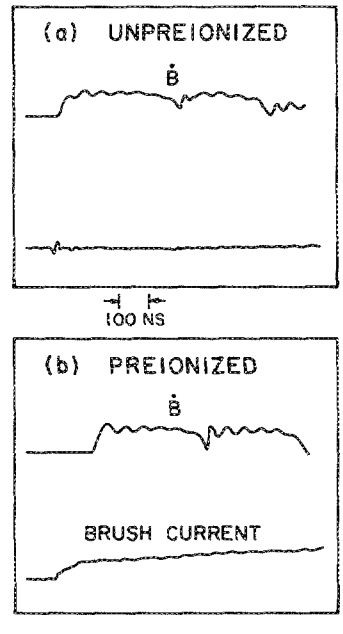

FIG. 5. B-dot traces for He implosions.

The free e^- line density (e^-/m in the z direction) is obtainable by simply integrating the shift for any given fringe of an interference pattern. For the four prominent fringes of Fig. 3(d), the average is $N_e = 4.5\times10^{19}$ m^{-1}. This gives $N_i = 2.3\times10^{19}$ m^{-1} for the ions; assuming, of course, that all the He atoms are stripped of both e^-'s at this point. This assumption can be justified based on the results of previous experiments on our machine.[8] It was found that He pinches seeded with 0.5% Kr (to allow for harder radiation) will radiate with the power spectrum peaked in the 200 eV range by the time the column reaches a radius of 0.7 cm. The secondary ionization energy for He is only 54 eV.

An independent estimate of N_i is based on the B-dot signal. This, as mentioned, gives the time t_p between the breakdown and pinch. The approximate relationship between the mass line density λ and t_p may be determined numerically by use of the 0-dimensional application of Newton's law to this geometry,

$$(2\pi R)P_m = -\lambda\frac{d^2R}{dt^2}. \tag{4}$$

Here, P_m is the external magnetic pressure $B^2/2\mu_0$ produced by the pinch current I and R is the plasma radius. Taking I to be the constant LC circuit response $I = I_m \sin\omega t$ (ignoring the time dependent plasma inductance), we have

$$\Lambda\rho\frac{d^2\rho}{d\tau^2} = -\sin^2\tau. \tag{5}$$

Here, $\rho = R/R_0$, $\tau = \omega t$, and

$$\Lambda = (4\pi\lambda/\mu_0)(R_0\omega/I_m)^2. \tag{6}$$

The function $\Lambda(\tau_p)$ relating Λ to the normalized pinch time τ_p for solutions of Eq. (5) $\rho_\Lambda(\tau)$ with initial conditions $\rho_\Lambda(0) = 1$ and $d\rho_\Lambda/d\tau|_{\tau=0} = 0$ [$\rho_\Lambda(\tau_p) = 0$] was numerically calculated for $\tau_p = 0.2$ to 2.0. $\epsilon(\tau_p)$, defined such that

$$\Lambda(\tau_p) = 0.113(1-\epsilon)\,\tau_p^4 \tag{7}$$

was thereby determined and is plotted in Fig. 6.

For the data presented, $\omega = 1.26\times10^6$ s^{-1}, $t_p = 380$ ns, $R_0 = 2$ cm, and $I_m = 0.45$ MA, resulting in $\Lambda = 5.5\times10^{-3}$ or $\lambda = 1.76\times10^{-7}$ kg/m. For He, this corresponds to $N_i = 2.6\times10^{19}$ m^{-1}, respectively close to the interferometer results. The nozzle has an annular opening of $W = 0.2$ cm resulting in a volume density of $n_i \approx N_i/2\pi R_0 W \approx 1\times10^{17}$ cm^{-3} here. The density at the anode will be much lower. No reliable data are available on the divergence of the gas leaving the nozzle. However, a rms atomic z vs r velocity ratio of 5 (optimistically high) would result in the gas wall thickening to 0.6 cm by the time the anode 1 cm away is reached. This would result in an anode gas density of $n_i \approx 3\times10^{16}$ cm^{-3}.

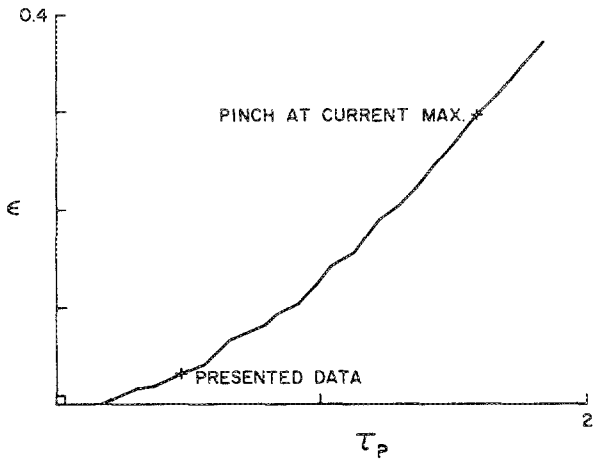

FIG. 6. Λ correction term ϵ vs τ_p.

Representation (7) was chosen because solutions $\rho_\Lambda^0(\tau)$ of the equation,

$$\Lambda\rho\frac{d^2\rho}{d\tau^2} = -\tau^2, \tag{8}$$

having the same initial conditions as ρ_Λ have the Λ vs τ_p relation,

$$\Lambda = \Lambda^0(\tau_p) = 0.113\,\tau_p^4. \tag{9}$$

The fact that $\Lambda \propto \tau_p^4$ follows directly from

$$\rho_\Lambda^0(\tau) = \rho_1^0(\tau/\Lambda^{1/4}), \tag{10}$$

which may be verified by substitution into Eq. (8). The constant 0.113 was found by numerically determining $\rho_1^0(\tau)$. Equation (8) corresponds to the case of $\tau_p \ll 1$ for which $\sin^2\tau \approx \tau^2$ may be used in Eq. (5). This, in turn, corresponds to a ramped pinch current $I = I_m\,\omega t$. Figure 6 shows that ϵ is small enough (0.03) for the data presented to use this approximation.

An estimate is made of the magnitude of the initial perturbations in the unpreionized gas columns that would be required to result in the R-T growth observed in Fig. 4(a). In our notation, the coupled equations of motion for radially symmetric linear perturbations $(\xi\bar{e}_r - i\eta\,\bar{e}_z)\,e^{ikz}$ of a thin incompressible cylindrical shell imploding as a result of an external field $B_\theta\bar{e}_\theta$ are

$$\frac{d^2\eta}{d\tau^2} = K\xi\frac{d^2\rho}{d\tau^2}, \tag{11a}$$

$$\frac{d^2\xi}{d\tau^2} = \left(K\eta - \frac{\xi}{\rho}\right)\frac{d^2\rho}{d\tau^2}, \tag{11b}$$

where $K = kR_0$. These are normalized forms of Eqs. (53) and (54) of Harris.[9] Using $\rho = \rho_\Lambda^0(\tau)$, consider solutions $\xi_\Lambda^0(\tau)$ and $\eta_\Lambda^0(\tau)$ with initial conditions $\xi(0) = 1$, $d\xi/d\tau|_{\tau=0} = \eta(0) = d\eta/d\tau|_{\tau=0} = 0$. Substitution into Eqs. (11a) and (11b) reveals that, by virtue of relation (10),

$$\xi_\Lambda^0(\tau) = \xi_1^0(\tau/\Lambda^{1/4}); \quad \eta_\Lambda^0(\tau) = \eta_1^0(\tau/\Lambda^{1/4}). \tag{12}$$

Since, for a given K, both ξ_Λ^0 and ρ_Λ^0 may be expressed as functions of $S = \tau/\Lambda^{1/4}$ alone, the function $\xi^0(\rho)$ relating ξ_Λ^0 to $\rho = \rho_\Lambda^0$ is independent of Λ. Numerical solutions were performed, and $\ln\xi^0$ vs ρ is plotted for various values of K in Fig. 7.

Corresponding solutions ξ_Λ and η_Λ of Eqs. (11a) and (11b) were found for the same range of K but using $\rho = \rho_\Lambda(\tau)$ with $\Lambda = 0.69$. This corresponds to a pinch at current max of a sinusoidal current rise. It was found that, even though ξ_Λ and ρ_Λ individually vary significantly from ξ_Λ^0 and ρ_Λ^0 ($\epsilon = 0.3$), the function $\xi(\rho)$, relating ξ_Λ to $\rho = \rho_\Lambda$, is almost identical to $\xi^0(\rho)$. $\ln\xi$ varies from $\ln\xi^0$ by

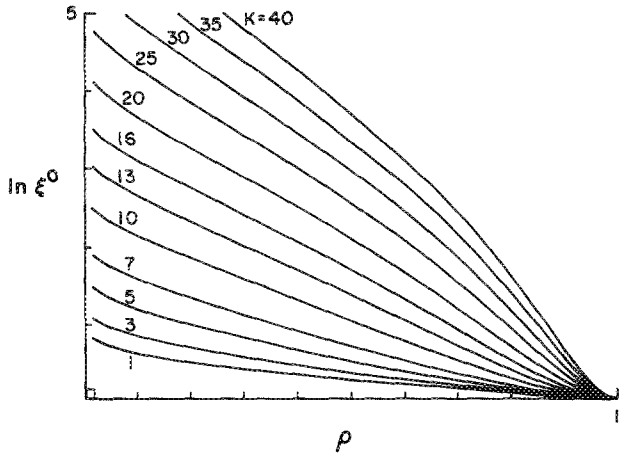

FIG. 7. Rayleigh–Taylor growth of radial perturbations.

no more than 2% for any given ρ. From this, it may be inferred that Fig. 7 should be a useful reference for any similar implosion geometry where the current rises in a smooth monotonic manner.

Figure 4(a) shows a perturbation with $k \approx 5\ \mathrm{cm}^{-1}$ at a radius of $R \approx 0.6$ cm. This gives $K \approx 10$, $\rho \approx 0.3$, and therefore $\xi \approx e^{1.7}$. Figure 4(a), therefore, theoretically shows a perturbation about five times the size of that initially resulting from the unpreionized breakdown.

Upon elimination of initial perturbations caused by low density breakdown by preionization, a larger scale-length (and therefore slower growing) instability becomes apparent resulting in the axial transport of mass toward the nozzle observed in Figs. 3(d)–3(f). This is presumably due to the fact that the capacitor bank must be fired before steady-state conditions are reached in the gas flow from the nozzle to avoid excessive background gas. The resultant positive time derivative of the gas flow rate results in a z-dependent mass line density. This effect has been treated in a recent paper[10] in terms of a thin axially symmetric imploding shell. In this reference, mass accretion and more general nonlinear evolution of the shell shape are assumed. Our simplified treatment based on Eqs. (11a) and (11b), however, indicates that a thin shell approach which ignores thermal instabilities is insufficient to account for the magnitude of the mass transport observed, at least at relative radii $\rho \leqslant 0.3$.

We assume a normalized line density at breakdown of the form $\Lambda = \Lambda^0 + \Lambda^1$, where Λ^0 is the average density between the anode and cathode ($z = 0, L$ at the anode, cathode, respectively), and

$$\Lambda^1 = \Lambda_z^1\left(z - \frac{L}{2}\right), \quad \Lambda_z^1 = \left.\frac{\partial \Lambda}{\partial z}\right|_{z = L/2}. \tag{13}$$

From mass flow continuity we have, to first order consistent with Eq. (13),

$$\frac{d\Lambda^0}{dt} - v\,\Lambda_z^1 = 0. \tag{14}$$

Here, v is the mean atomic velocity in the negative z direction averaged over r and θ is assumed constant. v may be estimated from the adiabatic equation for temperature T of an ideal gas with velocity v initial at rest with temperature T_0,[11]

$$T = T_0\left(1 - \frac{(\gamma - 1)mv^2}{2\gamma K T_0}\right). \tag{15}$$

Assuming low gas divergence and (therefore) temperature, we have

$$v = \left(\frac{2\gamma}{\gamma - 1}\right)^{1/2}\left(\frac{KT_0}{m}\right)^{1/2}. \tag{16}$$

Now consider the experimentally measured function $\tau_p(t)$ relating τ_p, as determined from B-dot signals, to the time delay t between the start of gas flow from the puff valve, as determined by the breakdown pin gas detector, and the capacitor bank trigger signal. From Eqs. (9) and (14) we have

$$\Lambda_z^1 = \frac{0.113}{v}\left(\frac{d\tau_p^4}{dt}\right). \tag{17}$$

Λ^1 is related to the prebreakdown fluid element perturbation in the z direction at breakdown ϵ^1 by the first-order one-dimensional continuity condition

$$\Lambda^1 + \Lambda^0\frac{\partial \epsilon_1}{\partial z} = 0. \tag{18}$$

With boundary condition $\epsilon^1 = 0$ at $z = 0$ and L we have, using Eq. (13),

$$\epsilon^1 = (\Lambda_z^1/2\Lambda^0)(Lz - z^2), \tag{19}$$

which has the Fourier series representation

$$\epsilon^1 = \frac{4L^2\Lambda_z^1}{\pi^3\Lambda^0}\sum_{n=1}^{\infty}\left(\frac{1}{2n-1}\right)^3 \sin\left(\frac{(2n-1)\pi z}{L}\right). \tag{20}$$

This expansion was chosen to assure that when time propagated by Eqs. (11a) and (11b), axial fluid displacements will be zero at the anode and cathode. These boundary conditions should be more appropriate at the nozzle than at the anode since the plasma will stagnate at the nozzle's solid surface but may move freely away from the anode.

As we are concerned primarily with bulk transport, we will consider only the dominant $n = 1$ term

$$\epsilon^1 = \frac{4L^2\Lambda_z^1}{\pi^3\Lambda^0}\sin\left(\frac{Kz}{R_0}\right), \quad K = \frac{\pi R_0}{L}. \tag{21}$$

Just as with $\eta^0(\rho)$ discussed earlier, for a given K, the function $\eta^1(\rho)$ relating solution $\eta_\Lambda^1(\tau)$ of Eqs. (13a) and (13b) to $\rho = \rho_\Lambda^0(\tau)$, but with initial conditions $\xi(0) = d\xi/d\tau|_{\tau=0} = d\eta/d\tau|_{\tau=0} = 0$, $\eta(0) = 1$, is independent of Λ. $\eta^1(\rho)$ is plotted for various K in Fig. 8. As with Fig. 7, Fig. 8 can be expected to be a useful reference for any implosion where the current rises in a smooth monotonic manner.

Under the single K-mode approximation Eq. (21) we have, by virtue of the linearity of Eqs. (11a), (11b), and (18), $\epsilon(\rho) = \epsilon^1\eta^1(\rho)$, $\Lambda(\rho) = \Lambda^0 + \Lambda^1\eta^1(\rho)$, and

$$\left.\frac{\partial \Lambda}{\partial z}\right|_{z = L/2} = \Lambda_z^1\,\eta^1(\rho). \tag{22}$$

Here, $\epsilon(\rho)$ and $\Lambda(\rho)$ are the functions relating the time-dependent fluid displacement and line density, respectively, to $\rho = \rho_\Lambda^0(\tau)$.

Several implosions were performed with the breakdown time delay t varying from 0.33 to 0.37 ms ($t = 0.35$ ms for the presented data) and τ_p^4 vs t was fit to a line. $d\tau_p^4/dt$ was

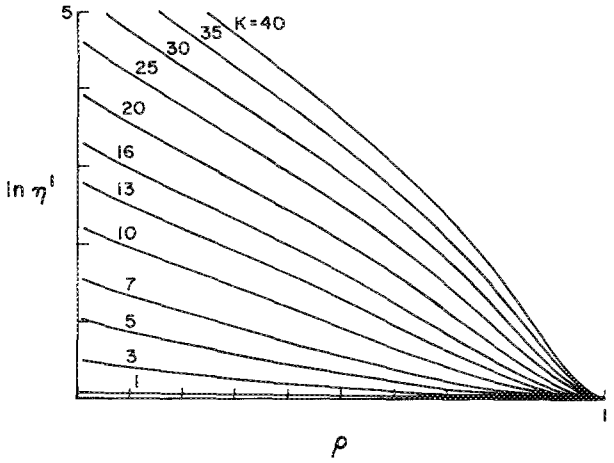

FIG. 8. Rayleigh–Taylor growth of axial perturbations.

thereby estimated to be $0.9\times10^{3}\ s^{-1}$ with, perhaps, as much as 30% error. With $T_0 = 300$ K, v for helium is, from Eq. (16) ($\gamma = 5/3$), 1.8×10^{3} m/s. From Eq. (17) $\Lambda_z^1 = 6\times10^{-2}\ m^{-1}$. With an A–K gap of $L = 1$ cm and $\Lambda^0 = 5.5\times10^{-3}$, this corresponds to a ± 0.5 variation in Λ from Λ^0.

For interferogram 3(d), $\rho = 0.3$. From Eqs. (21), (22), and Fig. 8 we have $K = 6$, $\eta^1 = 2$, and therefore $\partial\Lambda/\partial z = 1.2\times10^{-1}\ m^{-1}$ is predicted for 3(d). However, integration and comparison of the four prominent fringes of Fig. 3(d) reveal that $\partial\Lambda/\partial z = 5\times10^{-1}\ m^{-1}$. The disparity becomes worse for Figs. 3(e) and 3(f) since, from Fig. 8, $\partial\Lambda/\partial z$ should grow by no more than a factor of 3 from the initial value, or by a factor of 1.5 from the value at $\rho = 0.3$ [Fig. 3(d)].

As mentioned, Ref. 10 includes a treatment of the effects of mass accretion for an initial gas jet which, invariably, diverges as it leaves the nozzle. It is shown that this effect contributes to mass transport away from the nozzle and therefore cannot account for our discrepancy. In fact, in this reference, it is suggested that the harmful effects of gas divergence may be partially canceled by varying $\partial\Lambda/\partial z$ in the manner discussed. Nonlinear evolution, also treated in Ref. 10, is also an unlikely explanation since the factor of 3 growth in an initial ± 0.05 variation in Λ predicted should still lie in the linear regime. Apparently, a more general treatment of MHD thermally driven transport is necessary for a more quantitative description.

ACKNOWLEDGMENTS

This work was supported in part by Sandia National Laboratories. The primary author (E. R.) wishes to acknowledge Marco Cavenago for useful conversations.

[1] E. Bar-Avraham, A. Fisher, E. Mako, J. Peacock, and J. Shiloh, IEEE Trans. Plasma Sci. **PS-6**, 29.6 (1978).
[2] J. Shiloh, A. Fisher, and E. Bar-Avraham, Appl. Phys. Lett. **35**, 390 (1979).
[3] G. Schmidt, *Physics of High Temperature Plasmas*, 2nd ed. (Academic, New York, 1979), p. 93.
[4] A. Fisher, F. Mako, and J. Shiloh, Rev. Sci. Instrum. **49**, 872 (1978).
[5] R. Prohaska and A. Fisher, Rev. Sci. Instrum. **53**, 1092 (1982).
[6] K. L. Bell and A. E. Kingston, J. Phys. B Ser. 2, **2**, 1125 (1969).
[7] R. H. Huddlestone and S. L. Leonard, Eds., *Plasma Diagnostic Techniques* (Academic, New York, 1965), pp. 431–473.
[8] J. Bailey, Ph.D. thesis, University of California, Irvine, 1983, pp. 155 and 157.
[9] E. G. Harris, Phys. Fluids **5**, 1057 (1962).
[10] T. W. Hussey and M. K. Matzen, J. Appl. Phys. **59**, 2677 (1986).
[11] L. D. Landau and E. M. Lifshitz, Eds., *Fluid Mechanics* (Addison-Wesley, Reading, MA, 1959), p. 316.